ARTICLE IN PRESS

Available online at www.sciencedirect.com

ScienceDirect

Advances in Space Research xxx (xxxx) xxx

ADVANCES IN SPACE RESEARCH (a COSPAR publication)

www.elsevier.com/locate/asr

The Deep Space Radiation Probe: Development of a first lunar science payload for space environment studies and capacity building

Loren C. Chang [a,b,*], Wei-Yi Lin [a,b], Yi-Hsuan Chou [a,b], Jen-Siang Lin [a,b], Chieh Lung [a,b], I. Chen [a,b], Kai-Jie Hou [a,b], Glenn Franco Gacal [a,b], Yi-Chung Chiu [a,b], Yushun Wang [a,b], Hui-Hui Chou [a,b], Chi-Kuang Chao [a,b], Jann-Yenq Liu [a,b], Tung-Yuan Hsiao [c], I-Chun Cho [d,e,f], Takumi Date [g], Masayuki Urata [g], Masahiro Taeda [g], Kenichiro Tanaka [g], Nikola Vasovic [h], Niall Keegan [h]

[a] *Department of Space Science and Engineering, National Central University, 300 Zhongda Road, Zhongli District, Taoyuan City 320317, Taiwan*
[b] *Center for Astronautical Physics and Engineering, National Central University, 300 Zhongda Road, Zhongli District, Taoyuan City 320317, Taiwan*
[c] *Institute of Nuclear Engineering and Science, National Tsing Hua University, Section 2, Kuang-Fu Road, LTM Building Room 310, Hsinchu City, 300044, Taiwan*
[d] *Research Center for Radiation Medicine, Chang Gung University, No. 259, Wenhua 1st Rd, Guishan District, Taoyuan City 333323, Taiwan*
[e] *Institute for Radiological Research, Chang Gung University, No. 259, Wenhua 1st Rd, Guishan District, Taoyuan City 333323, Taiwan*
[f] *Radiation Research Core Laboratory, Linkou Chang Gung Memorial Hospital, No. 15, Wenhua 1st Rd, Guishan District, Taoyuan City 333011, Taiwan*
[g] *ispace. inc, 3F, 3-42-3 Nihonbashi Hamacho, Chuo-ku, Tokyo 103-0007, Japan*
[h] *Varadis, Carrigaline Industrial Estate, Unit 2, Site 13, Carrigaline, Co. Cork P43 DC53, Ireland*

Received 14 January 2024; received in revised form 14 May 2024; accepted 16 May 2024

Abstract

Regions outside of Low Earth Orbit (LEO, altitudes above approximately 1000 km) are classified as "deep space", including Medium Earth Orbit (MEO), geostationary orbit (GEO), as well as cislunar and lunar space. The deep space environment poses many challenges for human and robotic exploration, including stronger ionizing radiation fluxes, more extreme temperature variations, as well as limited data downlink volume. With the growth of the rideshare and hosted payload model aboard government and commercial lunar missions, developing the capacity to design and implement payloads and other space avionics for this environment is of increased importance this decade. Utilizing one of the growing number of rideshare opportunities offered by commercial lunar mission providers, National Central University (NCU) has been working on the rapid development of Taiwan's first scientific payload for lunar lander use, with launch aboard the HAKUTO-R Mission 2 (M2) lander from ispace, inc. scheduled not earlier than Q4 2024. This Deep Space Radiation Probe (DSRP) will provide measurements of radiation dose, dose rate, and single event upset (SEU) rate during the Earth-Moon transit, in lunar orbit, as well as on the lunar surface. DSRP utilizes elements of the on-board computer (OBC) developed and flight qualified aboard the NCU-developed IDEASSat 3U CubeSat mission in 2021, and was developed by a student team, in consultation with experienced engineers from the lunar lander team. In this paper, we will report on the objectives, concept of operation, design, and implementation of the DSRP project. We will also describe the steps taken to facilitate parallel development of the DSRP payload and the HAKUTO-R M2 lander, as well as lessons learned during the design, implementation, and qualification process. The radiation data

* Corresponding author at: Department of Space Science and Engineering, National Central University, 300 Zhongda Road, Zhongli District, Taoyuan City 320317, Taiwan.
E-mail address: loren@g.ncu.edu.tw (L.C. Chang).

https://doi.org/10.1016/j.asr.2024.05.032
0273-1177/

provided by DSRP will be beneficial for the development of future deep space spacecraft avionics, as well as crewed missions, and will also serve to build the capacity for deep space spacecraft and payload development at NCU.

Keywords: Lunar payload; Ionizing radiation; Single event effects; Deep space; Lunar lander

1. Introduction

Over the past ten years, the barriers to accessing space have been greatly reduced due to the proliferation of rideshare opportunities, as well as small satellites based on automotive, industrial, and even commercial grade hardware. Rideshare opportunities to Low Earth Orbit (LEO) for small satellites have led to the cost of deploying space platforms to a range affordable for educational institutions for scientific, education, and technology demonstration purposes (Baker et al., 2020; Millan et al., 2019). Hosted payloads, such as NASA's Global Observations of the Limb and Disc (GOLD) mission, have also opened regions beyond LEO to new players in space (Eastes et al., 2017). With the implementation of Project Artemis, as well as the growth in rideshare and hosted payload opportunities to higher orbits, such as Geosynchronous Transfer Orbit (GTO), and even cislunar and lunar space, the coming decade shows many new opportunities in developing and deploying space platforms into Deep Space (Desai et al., 2019).

Compared to LEO, several environmental and technical challenges exist for space platforms designed for and deployed into deep space. Long communication distances and much higher free space loss severely constrains the volume of data that can be returned, as well as the speed at which it can be downlinked. The farther distance from the eclipse region in the Earth's shadow results in longer extended times in direct sunlight, leading to greater challenges in thermal control (Wertz & Larson, 1999).

The ionizing radiation environment is one of the greatest environmental threats to spacecraft electronics and astronauts outside of LEO. Non-LEO orbits could have trajectories that pass through regions of high radiation flux, such as the trapped electron and proton populations of the Van Allen radiation belts inside the Earth's magnetosphere. When the spacecraft are in deep space outside of the Earth's magnetosphere they can be hit by Solar Energetic Particles and/or Galactic Cosmic Rays (GCRs) or dense and energetic plasma of the interplanetary Coronal Mass Ejection with no shielding from the Earth's magnetic field. The total ionizing dose absorbed by spacecraft electronics over the course of their mission duration can greatly reduce performance and lifetime. The impact of a single ionizing radiation particle also has the probability of causing single event effects (SEEs) that can lead to anomalous performance, as well as temporary or even permanent device failure (Langley et al., 2003; Rodbell et al., 2007; Baumann & Kruckmeyer, 2019). Prominent single event effects include single event upsets (SEUs), in which single or multiple bits stored in computer memory can be flipped via energetic particle impact. This can cause data corruption, as well as anomalous behavior and/or resets of on board flight software if the corrupted bits affect the control logic of flight software (Baker, 2000; Chiu et al., 2022). Single event latchups (SELs) can occur when complementary metal-oxide semiconductor (CMOS) devices are struck by heavy ions, forming a low impedance path supporting high currents between device power and ground, while also causing the device to lose functionality. SEL recovery can only occur if the device is power cycled and sustained overcurrent from SELs can result in device damage or destruction (Baumann & Kruckmeyer, 2019).

The measurement and characterization of ionizing radiation dose and dose rate in different space environments is thus important for the design and validation of spacecraft electronics to be operated in deep space, as well as for potential future human flights to the Moon. It has also been proposed that the counting of SEUs and measurement of SEU rates in spacecraft computer memory can also serve as a low-cost detector for ionizing radiation flux and dosage. By periodically performing Error Detection and Correction (EDAC) checks on saved data stored in memory, the accumulated number of SEUs can be counted, and the corrupted data reset in preparation for the next measurement cycle (Chen et al., 2019).

ispace, incorporated is a Japanese lunar exploration company that was initially formed in 2010 as part of an effort to compete for the Google Lunar X Prize, but later grew to provide commercial lunar payload delivery services. In the following paper, we describe the concept of operation, design, and implementation of a low-cost Deep Space Radiation Probe (DSRP) that was rapidly developed by NCU over a two-year period for use aboard the HAKUTO-R M2 lander developed by ispace, incorporated (Maltagliati, 2023; ispace inc., 2023a,b), as well as lessons learned during this process. Key challenges included parallel development of the DSRP payload in Taiwan at the same time as the HAKUTO-R M2 lander by ispace in Japan, lack of prior experience at NCU in designing payloads and spacecraft for deep space, limited development time, as well as the more severe mass and power constraints, vibration, thermal, and ionizing radiation conditions compared to past LEO missions developed at NCU (Lin et al., 2017; Duann et al., 2020; Chandran et al., 2021; Chiu et al., 2022). Preliminary contacts between

NCU and ispace were established in April 2021, with a formal Payload Services Agreement signed in March 2022. Prototype development of DSRP began in summer 2021, with an engineering model (EM) fit check performed with the HAKUTO-R M2 lander payload interface in February 2023. The DSRP flight model (FM) was delivered to ispace for integration with the HAKUTO-R M2 lander in December 2023 with an expected launch not earlier than 2024 Q4. The payload is also being modified for future LEO and deep space missions.

2. Mission scope and concept of operations (ConOps)

Following launch and initial check-out, the HAKUTO-R Mission 2 lunar lander will enter a low energy Earth-Moon transit orbit, during which DSRP will be powered on and begin scientific observations. This will be followed by Earth-Moon transit, lunar orbit, landing, and lunar surface operation. Barring any anomalies, DSRP will be active during the passive stages of the mission. The Science Traceability Matrix (STM) for DSRP is shown in Table 1, as formulated for inclusion aboard the ispace HAKUTO-R Mission 2 lunar lander with launch scheduled no earlier than Q4 2024. There are two scientific objectives (S1, S2) and one mission objective (M1). The science objectives of DSRP are to respectively measure the radiation dose and dose rate (S1), as well as to measure the SEU rate (S2) during Earth-Moon transit and on the surface of the Moon. The expected mission duration is for up to four months, with Earth-Moon transit and lunar orbit taking up to two months each, with up to 12 days of alive time on the lunar surface. In addition to periodic sampling of the measured radiation dose and SEU count, ancillary data needed to infer dose and SEU rates include time stamps for each sample, temperature, as well as orbit and absolute time knowledge in order to infer the location at which each sample was taken. Sampled science data, as well as periodic housekeeping (HK) data, are stored on the internal NAND flash memory of DSRP and can be played back to the spacecraft on command for downlink back to Earth. As a safeguard to monitor data corruption from SEUs, data stored in NAND Flash is protected using CRC16-CCITT error detection codes per ispace requirements. An additional mission objective is to design, implement, and qualify a deep space payload using a student team from NCU (M1). This is in the context of student education, as well as developing the capacity and know-how on the design, implementation, and qualification of payloads and spacecraft avionics intended for use outside LEO. Up to the end of 2023, all spacecraft and payloads from Taiwan have been confined to LEO, with the maximum altitude attained being that of the FORMOSAT-2 spacecraft operated by the Taiwan Space Agency (TASA, formerly the National Space Organization or NSPO), which operated in an 888 km altitude circular orbit from 2004 to 2016 (Chern et al., 2006).

DSRP contains two sensors to measure radiation dose and SEU count. Radiation dose is measured using a

Table 1
DSRP Science Traceability Matrix.

Deep Space Radiation Probe Mission Goal

The radiation environment is a hazard that must be faced by spacecraft avionics and human spaceflight, especially in the deep space environment. Knowledge of the radiation dose and dose rate in different space regions will help in quantifying this risk. The development of a robust payload capable of performing such measurements in deep space will also help in building capacity at National Central University (NCU) to develop radiation tolerant avionics suitable for deep space operation.

Science Traceability Matrix

Science (S) and Mission (M) Objectives	Objectives Measurement	Measurement Requirements (Capabilities)	Instrumentation	Instrument Requirements (Capabilities)	Data Processing Requirements (Capabilities)
S1. Measure the radiation dose and dose rate during Earth-Moon transit and on the surface of the Moon. S2. Measure the Single Event Upset (SEU) rate during the Earth-Moon transit and on the surface of the Moon. M1. Design, implement, and qualify a deep space payload using a student team at NCU.	Radiation dose and dose rate. SEU Rate Sampling period: 1 s–30 min. Continuous Operation Measurements from Low Earth Orbit to Earth-Moon transit and lunar surface. In-situ measurements aboard deep space vehicle. Observations for up to 4 months.	Sampling period: 2–30 min. Orbit Knowledge Absolute Time Knowledge Instrument Temperature Earth-Moon Transit: Up to 2 months. Lunar Orbit: Up to 2 months. Lunar Surface: Up to 12 days.	Deep Space Radiation Probe (DSRP): RADFET Dosimeter NAND Flash	Power: <0.9 W Maximum Data Rate: 600 bps Total Ionizing Dose Tolerance: 10 krad. Dose Resolution: 0.3 mrad/day	User Data Telemetry (Science Data Packet) + HK Packet 27 bytes + 47 bytes Onboard Storage (4 months of data, assume 15 s sample rate): 51.15 MB Instrument Temperature Absolute Time Knowledge

commercial off the shelf (COTS) Varadis VT-01A radiation sensitive field-effect transistor (RADFET) module, complete with readout circuit (Varadis, 2022). A RADFET is a passive MOSFET-based sensor that has a threshold voltage that is sensitive to integrated ionizing radiation dosage. By measuring the change in RADFET threshold voltage ($V_{threshold}$), the absorbed ionizing radiation dose can be inferred based on laboratory calibration data. RADFETs have the benefit of being a passive sensor whose change in threshold voltage due to irradiation is not dependent upon being powered on (Andjelkovic et al., 2022). By sampling the RADFET threshold voltage at specified and tagged time intervals, the dose rate can be inferred from the collected data through post processing.

DSRP includes commercial off the shelf NAND flash memory to serve as a sensor for SEUs, while also serving as non-volatile memory for storage for periodically logged science and HK data. NAND flash is highly attractive due to its low power requirements and high memory density. However, even without the effects of ionizing radiation, bit errors can occur due to data retention errors, as well as disturbances from read/write operations. The use of EDAC is therefore recommended when using NAND flash, with codes capable of single error correction and double error detection (SECDED) per word considered to be sufficient for the purposes of single level cell (SLC) NAND flash. It is notable that disturb errors tend to be rarer in SLC NAND flash devices compared to multi-level cell (MLC) devices, hence SLC NAND flash is selected for DSRP (Heidecker, 2012; Fabiano & Furano, 2013). In this case, the NAND flash used for DSRP was the MT29F128G08AJAAAWP-ITZ from Micron Technology (Micron Technology, Inc., 2023). A section of memory blocks allocated to the SEU counting experiment are preprogrammed with known Bytes and will be periodically scanned to count the rate at which SEUs occur.

Science data packets containing time tagged RADFET threshold voltages and SEU counts have a size of 27 bytes, while HK packets containing information such as time tagged command counts, reboot counts, write pointers, and electrical data will take 47 bytes. Both science and HK data are logged at a maximum cadence of 15 s. Assuming a mission duration of 4 months, this results in a data storage requirement of 51.15 MB. The NAND flash size of 16 GB used in DSRP is more than sufficient to satisfy this data storage requirement, while leaving plenty of margin, as well as space for the SEU counting experiment. Additional constraints on DSRP include power consumption less than 0.9 W, and a mass less than 400 g. DSRP must also be capable of withstanding a total ionizing dose (TID) of 10 krad, as specified by ispace.

The ConOps of the DSRP payload software is shown in Fig. 1. Upon boot up, the payload will boot into Science mode, while periodically generating and logging Housekeeping (HK) data packets containing payload state of health data, as well as the last logged science data. The HK packets are generated and returned to the host spacecraft upon request and are also saved to payload Flash memory for future recall. DSRP also accepts a time synchronization signal from the spacecraft to set its internal clock to spacecraft system time, which can be used to infer the position of the spacecraft during postprocessing of payload data. In Science mode, the payload controller will read the threshold voltage from the RADFET. It will then scrub all the packets in NAND Flash allocated to the SEU count experiment, identifying packet errors by determining which packets have deviated from a nominal value of 0xFF. Packets failing this test will be reset, and the SEU count incremented by the number of bits in error. After finishing the sweep, the RADFET threshold voltage and SEU bit error count are saved to DSRP NAND Flash as a new science data packet that can be recalled upon command by the host spacecraft.

It is noted that the logical state of a NAND Flash bit is determined by the value of its threshold voltage relative to the read voltage, with a lower (higher) threshold voltage corresponding to a logical "1" ("0"). 0xFF is the erased state of a NAND Flash byte, corresponding to 8 bits with logical "1". Research has shown that additional ionization from a heavy ion strike may create excess holes in the floating gate that would recombine with electrons if they are present, decreasing the threshold voltage. If the resulting threashold voltage is lower than the read voltage, the strike does not create a bit-flip visible in the readout. Upon the next erase cycle, holes are retained until the logical value of "0" is written (Sheng et al., 2024). For future revisions of DSRP, the default value of the scrubbed bits will be modified to a logical "0" to eliminate this source of uncertainty.

The most recent RADFET threshold voltage and bit error counts are also provided to the host spacecraft with HK data packets, which are generated and transmitted to the spacecraft for archival at a 15 s cadence. Bulk replays of science data packets stored in DSRP NAND Flash are also available as a backup option for science data retrieval.

3. Payload architecture and design constraints

To facilitate the parallel development of DSRP by the NCU team along with the HAKUTO-R M2 lander, an Interface Requirement Document (IRD) specifying the mechanical, electrical, data, and thermal interface requirements between DSRP and the lander was issued at the time of official project kickoff in March 2022. DSRP was assigned an installation on the top panel of the HAKUTO-R M2 lander with direct exposure to space. Notable development constraints and specifications are shown in Table 2. DSRP was subject to significant power, mass, and volume constraints with a maximum power consumption not to exceed 900 mW, mass cap of 400 g, and volume not to exceed 150 × 150 × 40 mm (approximately 0.3–0.4U). It is notable that the mass and volume constraints included the payload electronics, chassis, fasteners, and thermal control components such as multilayer insula-

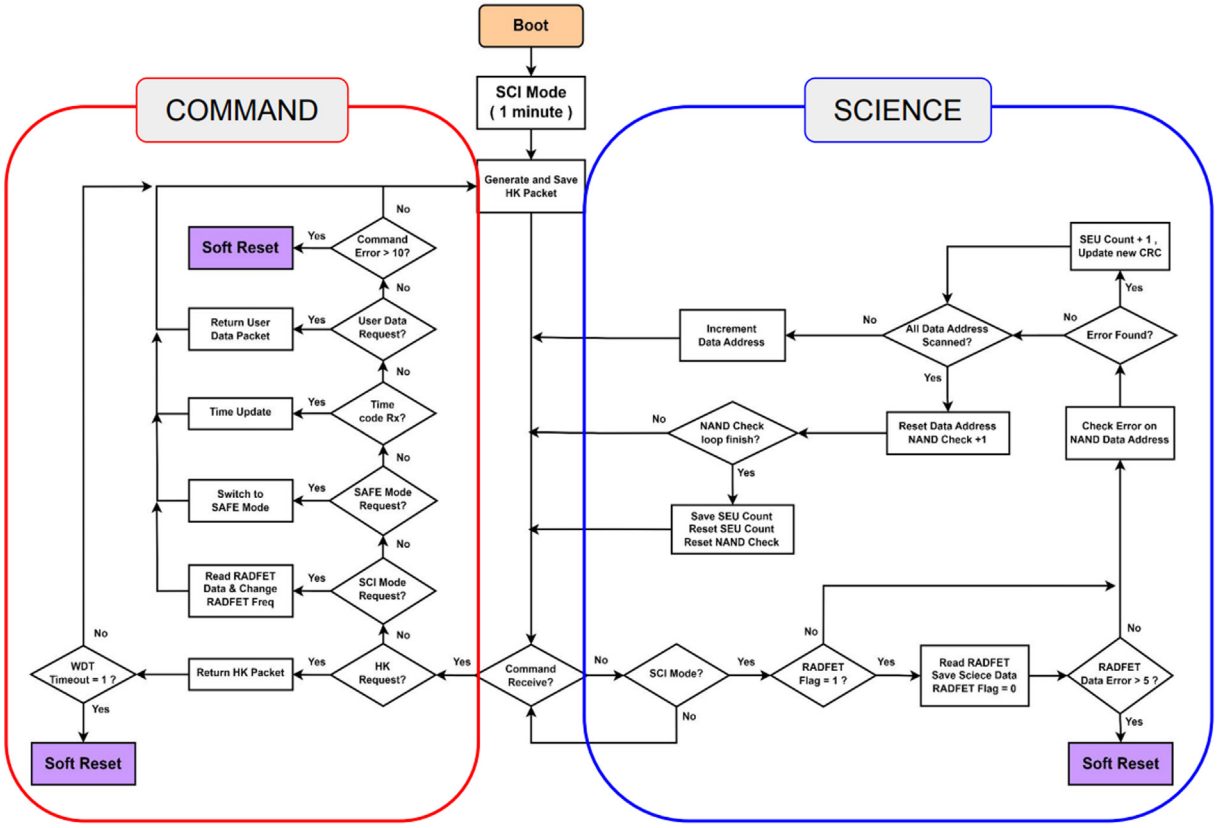

Fig. 1. DSRP payload embedded software concept of operation.

Table 2
DSPR Interface Requirements.

Electrical Power Input	5 V, 12 V
Maximum Power Consumption	900 mW
Maximum Payload Mass	400 g
Maximum Envelope	150 × 150 × 40 mm
Data Interface Protocol	RS-422
Baud Rate	921,600 bps
Survivable Total Ionizing Dose	10 krad with 1 mm aluminum shielding
FM Delivery Deadline	December 2023

tion (MLI). DSRP was also required to be capable of surviving a total ionizing dose (TID) of 10 krad behind 1 mm of aluminum shielding. A flight model delivery deadline of December 2023 provided the payload team of approximately 21 months of development, implementation, and verification time for DSRP.

A block diagram of the hardware architecture of DSRP is shown in Fig. 2, which illustrates the main electrical and data interfaces between the powered subsystems comprising DSRP, as well as with the HAKUTO-R lander payload interface card (PIF). The PIF provides the electrical and data interface between the lander and DSRP. The powered subsystems of DSRP are the electrical interface, data interface, payload controller, RADFET readout module, and NAND Flash chip. These powered components are de-rated according to NASA EEE-INST-002 guidelines to increase lifespan (NASA, 2003). Not shown are the structural and thermal control subsystems, which are respectively comprised of the payload chassis and fasteners, as well as thermal insulation, radiators, and heat conductors.

The DSRP electrical interface is interfaced with regulated 5 V and 12 V power supplies from the lander PIF. DSRP electrical and digital ground connections are also interfaced with the PIF ground. A 3.3 V DC/DC buck converter further converts the 5 V input power to the 3.3 V required by most of the payload electrical components, except for the RADFET readout module, which requires 12 V input. eFuses are installed along the 5 V and 12 V power input busses to provide an autonomous recovery mechanism from single event latchups (SELs), which can cause high electrical currents and device incapacitation that can only be removed by power cycling (Baumann & Kruckmeyer, 2019). In the event overcurrent is detected by the eFuse, the eFuse will temporarily disconnect the power bus, allowing for power cycling and SEL recovery to occur.

The DSRP data interface consists of an RS-422 transceiver IC and supporting circuits, which converts between the universal asynchronous receiver/transmitter (UART) interface protocol of the payload controller and the 921,600 bps RS-422 protocol required by the lander PIF.

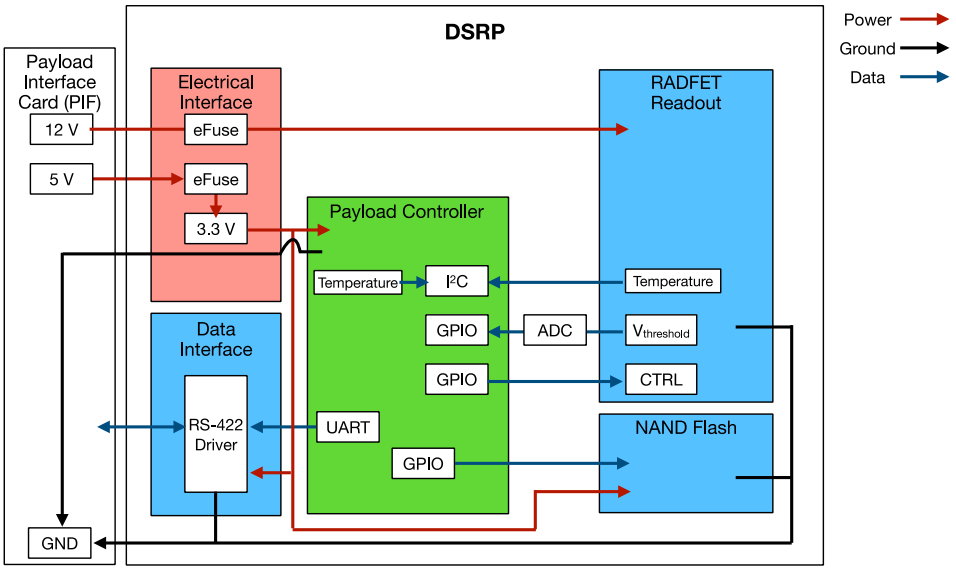

Fig. 2. DSRP hardware architecture. Red arrows correspond to power interfaces, black arrows correspond to ground, blue arrows correspond to data interfaces.

The payload controller of DSRP is a system on module (SOM) unit from Emcraft based on the Microsemi SmartFusion2 system on chip (SoC) (Microchip Technology, Inc., 2023), which is responsible for sensor readout and control, NAND flash read/ write, as well as communication with the spacecraft for command reception and telemetry transmission. Although not explicitly intended for space-based applications, the behavior of the SmartFusion2 in ionizing radiation environments has been characterized, demonstrating a limiting total ionizing dose exposure between 480 and 660 Gray (48–66 krad) and reduced SEE sensitivity if Triple Modular Redundancy (TMR) is utilized (Microsemi, 2014; Tsiligiannis & Danzeca, 2017). The SmartFusion2 was utilized successfully as on-board computer (OBC) for the IDEASSat 3U CubeSat (Duann et al., 2020; Chiu et al., 2022), as well as for the INSPIRESat-1 9U small satellite (Chandran et al., 2021), providing a Cortex M3 microprocessor for execution of embedded C code, as well as an FPGA fabric that can be utilized to implement interface protocols or serve as additional memory. The payload controller has data and control interfaces with the Varadis RM-VT01-A readout module, allowing for measurement of the RADFET threshold voltage from which the ionizing radiation dose can be derived using an analog to digital converter (ADC). Another data interface with the NAND Flash chip allows the payload controller to read and write data for future replay, as well as to scrub the blocks allocated to the SEU counting experiment. The payload controller also periodically polls temperature sensing circuits comprised of thermistors and ADC readout circuits to gauge the temperature of itself and the RADFET readout module, the latter of which can cause non-radiation related fluctuations in RADFET threshold voltage.

As mentioned previously, DSRP utilizes a COTS Varadis RM-VT01-A RADFET readout module, which provides buffered readout of threshold voltages from two identical RADFETs, designated R1 and R2. The RM-VT01-A also accepts control logic signals to select either R1 or R2 for readout, as well as an irradiation mode that is the default state in DSRP when threshold voltage measurement readouts are not being performed (Varadis, 2022).

The electrical components of DSRP are mounted on a single PCB board. The DSRP FM PCB board mounted in the bottom half of the payload chassis, including the RADFET and SmartFusion2 modules, is shown in Fig. 3a. A micro-D socket connector at the bottom center of Fig. 3a serves as the data and electrical interface to the spacecraft, while a JTAG connector on the upper right hand corner of the PCB is used for firmware updates and debugging. Fig. 3b shows DSRP fully enclosed in the chassis, complete with exposed cover painted with UV resistant white paint to serve as a radiator and MLI covering the remainder of the payload chassis, as well as the harness used to connect the payload micro-D socket connector and the HAKUTO-R PIF. The payload coordinate system is denoted in Fig. 4, which shows are rendering of the DSRP payload with MLI removed. The xy-plane corresponds to the length and width of the payload, while the z-axis is perpendicular to the payload base, with the chassis cover being on the +z face.

4. Payload design and analysis

4.1. Thermal design

DSRP is mounted on the top panel of the HAKUTO-R M2 lander, directly exposed to space. One of the challenges in the implementation of DSRP was the need to ensure that all the components of the payload remain within their

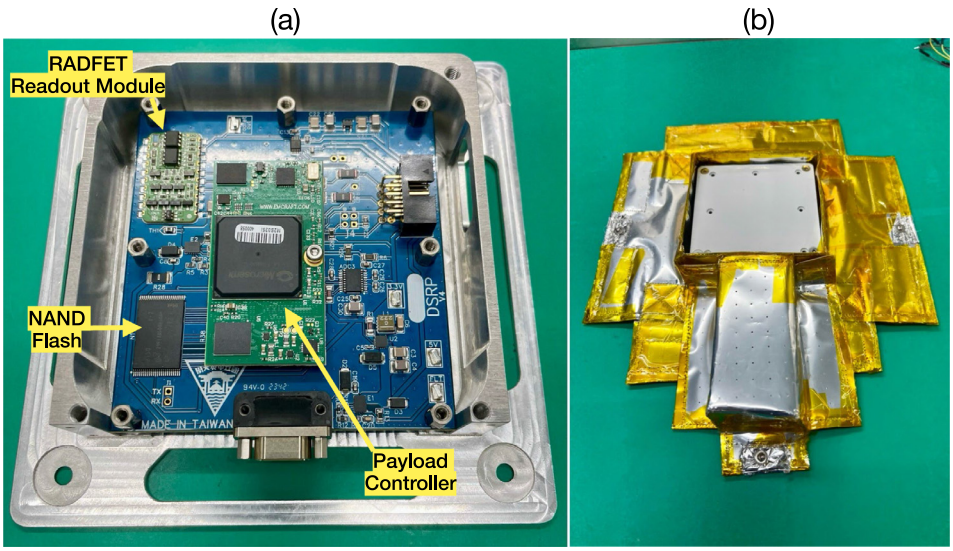

Fig. 3. (a) DSRP FM with payload chassis cover and MLI removed. (b) DSRP FM fully enclosed in chassis with MLI.

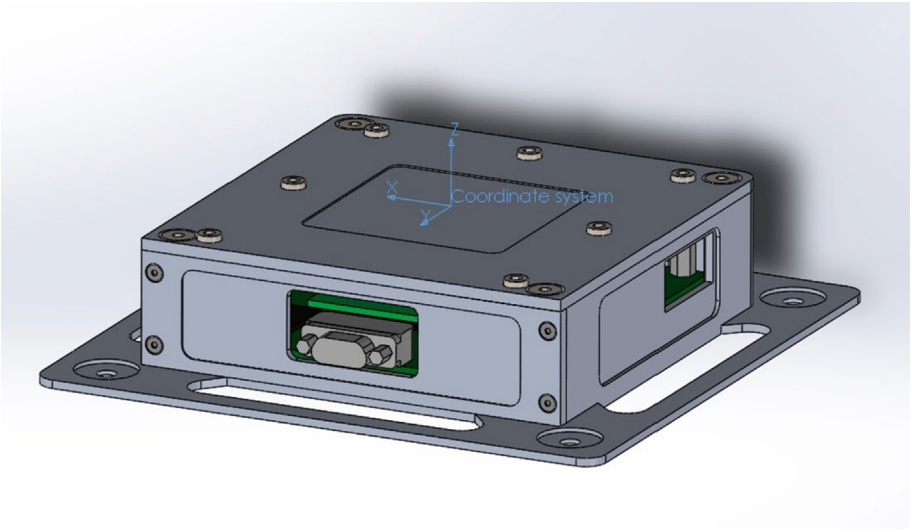

Fig. 4. Rendering of DSRP payload with LI removed and payload coordinate system indicated.

operational temperature ranges, while ensuring that the total payload mass remained within 400 g and the total power consumption remained within 900 mW. This was further complicated by the fact that compared to the dynamic heating conditions of lower Earth orbits where spacecraft pass between orbital segments in sunlight and eclipse, the low energy Earth-Moon transit orbit to be utilized by HAKUTO-R M2 is subject to relatively static heating conditions (Wertz & Larson, 1999). As a result, portions of the spacecraft facing the Sun will be subject to continuous heating, while portions of the spacecraft continuously facing cold space will be subject to continuous radiative cooling, leading to larger temperature extremes.

The boundary temperatures for portions of the lander top panel adjacent to DSRP were provided to the payload team by ispace for thermal simulation purposes. The portions of the lander in direct thermal contact with DSRP are the MLI covering this exterior portion of the spacecraft, as well as the lander top panel itself located beneath the MLI. The top panel MLI is in direct contact with the baseplate on the $-z$ face of DSRP, while the fasteners used to secure DSRP to the lander are in contact with the lander top panel beneath the MLI.

Thermal simulations for DSRP worst case hot and worst case cold conditions were performed using the commercially available Thermal Desktop analysis software (Mitchao et al., 2018). Under hot conditions for both the on orbit and lunar surface simulations, all electrical components on DSRP were powered on, ultimately dissipating consumed electrical power as waste heat. On orbit, the Sun

was assumed to be 5 degrees off the DSRP y-axis. On the lunar surface, the Sun was assumed to be 45 (90) degrees off the DSRP z-axis for worst case hot (cold), corresponding to a landing site of approximately 60 (75) degrees latitude. For cold conditions on orbit, DSRP was not powered on and dissipating waste heat, corresponding to scenarios where the payload might be powered off due to anomalies or other system level needs. For cold conditions on the lunar surface, DSRP was powered on and dissipating waste heat. Both on orbit cold cases, as well as the lunar surface hot case correspond to the steady state radiative equilibrium temperatures of the payload under the aforementioned conditions.

From the worst case hot simulation results in Table 3 without internal payload thermal control (TC) components, it can be seen that electronic components with high duty cycles such as the RS-422 transceiver can approach or exceed their maximum operating temperature limits, especially on the lunar surface due to the solar angle. We note that this, as well as other components selected for use with DSRP were automotive or industrial grade, owing to the higher cost and longer turnaround times of space and military grade components, as well as the CubeSat heritage of the design team, which emphasizes part selection and testing on a moderate budget (Sinclair & Dyer, 2013). In worst case cold conditions on orbit with no TC, the converse is true with most electrical components approaching or exceeding their minimum operating temperature limits, due in part to their being powered down and not dissipating waste heat. Under worst case cold conditions on the lunar surface with the electronics powered on, the high duty cycle RS-422 transceiver remains at elevated temperatures due to its inability to effectively dissipate waste heat, while other electrical components with lower duty cycles or power consumption remain at lower temperatures.

To remedy these problems, thermal tape was applied to the RS-422 transceiver to conduct heat away from this component to the inside of the payload chassis. An additional screw was also applied to the SmartFusion2 payload controller connecting it to the payload chassis to serve as a heat sink. As shown previously in Fig. 3b, the chassis cover was painted white using UV resistant paint to serve as a radiator, while the other external surfaces are covered with 12 layer MLI to aid in heat retention. DSRP is also separated from direct contact with the MLI covering the top panel of the lander through the use of four thermal collars installed at the holes for fasteners located on the corners of the baseplate of the payload chassis as shown in Fig. 5. Comparing the worst case hot results from the on orbit and lunar surface stages with and without TC components in Table 3, it can be seen that the temperature of the electrical component most prone to overheating, the RS-422 transceiver, has been reduced to within the safe operating range of the component. The overall temperature of DSRP is higher for the worst case hot simulation on the lunar surface compared to the worst case hot simulation on orbit, which reflects the larger cross sectional area of the payload

Table 3
Thermal Desktop simulation results for DSRP with and without thermal control (TC) components during on orbit and lunar surface mission stages.

Component (Operating Temperature Range, °C)	On Orbit Temperature (°C)				Lunar Surface (°C)			
	Worst Hot, no Thermal Control	Worst Hot, with Thermal Control	Worst Cold, no Thermal Control	Worst Cold, with Thermal Control	Worst Hot, no Thermal Control	Worst Hot, with Thermal Control	Worst Cold, no Thermal Control	Worst Cold, with Thermal Control
MLI	x	48	x	−32	x	65	X	−46
Chassis Body	60	47	−28	−32	75	65	−43	−46
Top Panel	60	48	−28	−32	75	65	−43	−46
Micro-D Connector	53	48	−40	−35	69	66	−64	−52
PCB and Misc. Electronics (−40 to 85)	56–101	45–60	−35 to −28	−32	78–89	65–71	−80 to −25	−47 to −29
RS-422 Transceiver (−40 to 80)	101	51	−28	−32	108	65	76	−45
RADFET (−40 to 85)	65	51	−28	−32	78	66	−38	−38
NAND Flash (−40 to 85)	67	52	−28	−32	82	70	−37	−51
SmartFusion2 SoC (−40 to 100)	68	54	−28	−32	82	70	−35	−41

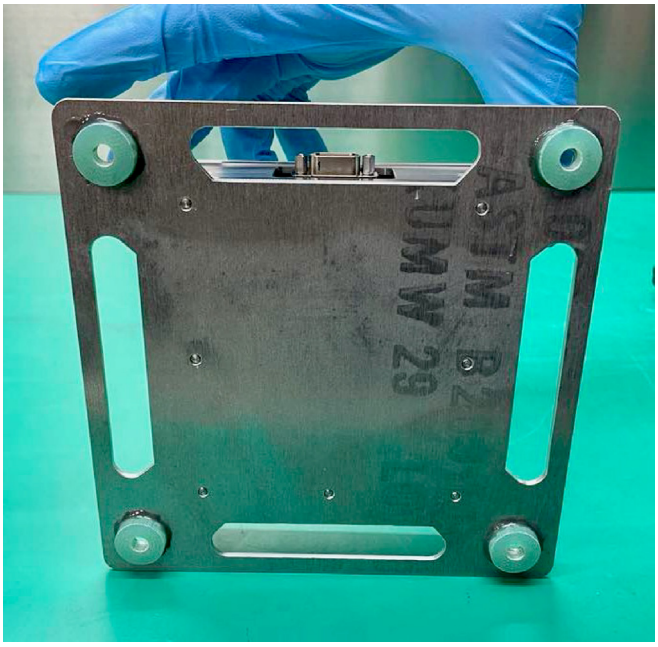

Fig. 5. Thermal collars installed to the baseplate of the DSRP payload chassis.

exposed to the Sun due to the angle of the Sun vector at this stage.

The aforementioned TC measures do have the effect of further reducing the worst case cold temperatures of several of the internal electrical components and chassis compared to the case without TC, due to the increased effectiveness in conducting heat away from internal components and radiating waste heat into space. Due to the inability to mitigate the sub-zero worst case cold internal temperatures of DSRP electronics using only internal payload TC components, an external heater will also be installed to the baseplate of DSRP by ispace that will be activated when the temperature of DSRP falls below 0 degrees Celsius, thereby addressing the worst case cold conditions. It should be noted that the heater is applied on the lander side and was not incorporated in the above simulations performed by the DSRP development team, as such information is considered proprietary to ispace and was performed by the lander team.

4.2. Structural design

The structural design of the DSRP payload is required to be capable of surviving the vibration, shock, and inertial loads of the HAKUTO-R M2 launch, course correction burns, and lunar landing. It is notable that the vibration and acceleration environment for this mission are considerably harsher compared to those encountered by many small satellites in Low Earth Orbit. The maximum static load factor required for DSRP to survive is 33 g along the z-axis and 30 g along the xy plane. Here, the load factor $g = 9.8\ m\ s^{-2}$. This can be compared with the maximum predicted lateral load factor of 17 g specified for CubeSat dispensers aboard the SpaceX Falcon 9 by Version 9 of the Rideshare Payload User's Guide (SpaceX, 2023). Additionally, the entire payload mass must be compliant with the 400 g mass limit allocated for DSRP.

The dimensions of the baseplate of the DSRP enclosure are 140 mm by 140 mm, while the overall height is 38.3 mm. The sides of the payload enclosure and the chassis cover were also subject to light weighting by reducing the thickness of the interior areas of these components, while the baseplate had holes cut out away from load bearing areas. As shown previously in Fig. 3, the DSRP payload PCB board is mounted inside a chassis machined from aluminum alloy 6061-T6 using seven standoffs and M3 screws. This is required to provide the necessary stiffness and strength to survive the mechanical loads of the flight environment. The Microsemi SmartFusion2 SOM used as payload controller is also secured to the chassis using an additional screw, which also serves to conduct heat away from this component. All fasteners and connectors were epoxied for the DSRP EMs and FM.

An unexpected lesson learned was encountered in the process of baking out an earlier revision of DSRP to ensure faster curing of the epoxy used to secure fasteners. Fig. 6a shows the initial layout used for the fasteners used to secure the PCB and payload controller to the chassis. In this configuration, the payload controller is secured to the chassis cover using a nut and bolt, which is the third fastener from the left denoted by the red oval. During the bake out, it was found that the PCB became warped with the center of the PCB bending upwards, as can be seen in Fig. 6b. This was determined to be the result of both differences in the heat conducted by the different fasteners, as well as the upward stress imposed by the nut and bolt securing the payload controller to the chassis cover. This fault was mitigated by securing the payload controller to the baseplate instead using a screw, as shown by the red oval in Fig. 6c. This removed the upward stress of the previous configuration and was found to be effective in preventing PCB warping during bake outs and thermal vacuum testing, as will be discussed in more detail in Section 5.3.

Structural analysis of DSRP was performed through analysis using SolidWorks, under conditions consistent with the flight environment specified in the IRD for static acceleration, random vibration, sinusoidal vibration, and shock. The specifications of the prescribed random vibration test used for DSRP are shown in Table 4, which also shows the maximum predicted environment (MPE) levels prescribed by the SpaceX Rideshare Payload User Guide for comparison (SpaceX, 2023). Plots of the two power spectral density (PSD) profiles are also shown in Fig. 7. The power spectral density (PSD) of the DSRP random vibration spectrum is increased from an initial value of 0.026 g^2/Hz by 6 dB/octave between 20 and 50 Hz, then held constant at 0.16 g^2/Hz between 50 and 800 Hz. The PSD is then decreased by 6 dB/octave between 800 and

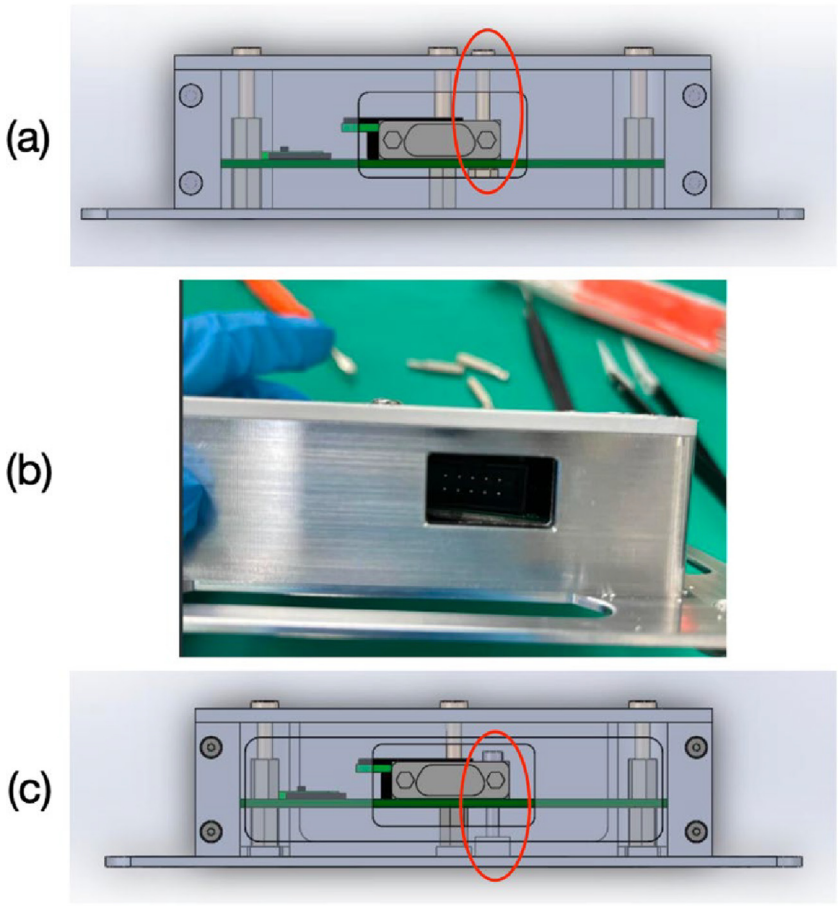

Fig. 6. (a) Initial layout of fasteners used to secure DSRP PCB to payload chassis. (b) Warped PCB resulting from bake out of initial fastener layout. (c) Revised fastener layout used in DSRP FM to prevent PCB warping when heated. Altered fastener marked by red oval.

Table 4
Random vibration qualification test specifications as used with DSRP compared with SpaceX Rideshare maximum predicted environment levels.

DSRP Test Levels		SpaceX Rideshare Maximum Predicted Environment	
Band (Hz)	DSRP Power Spectral Density (g^2/Hz)	Band (Hz)	Power Spectral Density (g^2/Hz)
20	0.026	20	0.01
20–50	+6 dB/octave	20–50	+1.33 dB/octave
50–800	0.16	50–700	0.015
800–2000	−6 dB/octave	700–800	+15.63 dB/octave
2000	0.026	800–925	0.03
		2000	0.00644
Overall GRMS	14.1 g	Overall GRMS	5.57 g

2000 Hz. The overall g-force level defined by the GRMS (root mean square) was 14.1 g. This GRMS is notably larger than the 5.57 g for the SpaceX Rideshare MPE, which also displays smaller amplitudes throughout this band.

The structural displacement of DSRP under the random vibration conditions predicted by SolidWorks is shown in Fig. 8. A maximum displacement of 3.76×10^{-2} mm occurs with the micro-D connector that serves as the data and electrical interface between DSRP and the HAKUTO-R M2 lander. This, as well as the results of the other simulations used in structural analysis, was within the maximum allowable value for this component, verifying that the DSRP structure can survive the expected flight environment and providing additional confidence before fabrication and testing of the DSRP EM and FM. DSRP does not include any internal harnessing, with the only harness being an external harness interfacing DSRP with the lander. Simulation of the effects of this harness were performed on a system-wide level and were beyond the scope of the DSRP payload team.

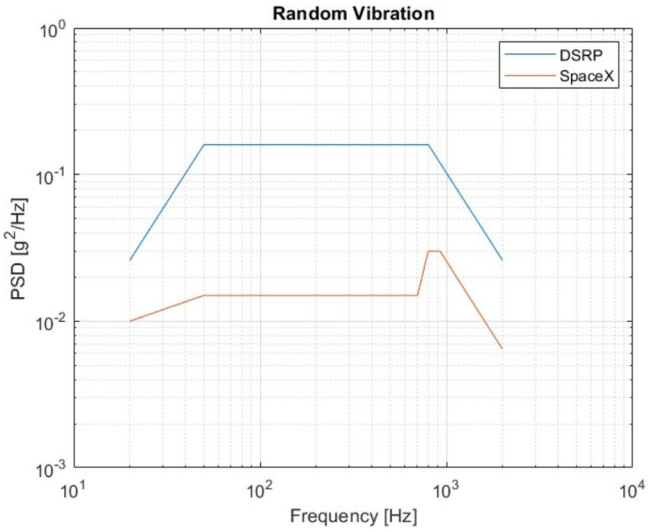

Fig. 7. Random vibration power spectral density for DSRP (blue line) and according to SpaceX Rideshare Payload User Guide (orange line).

5. Payload implementation and verification

5.1. Development progression

DSRP was designed and implemented by a core team of undergraduate and masters students at NCU with a size not exceeding four individuals. Some work handover was necessary due to student graduation during the project. Additional support and advising was provided by the faculty advisor, a postdoctoral researcher, lab staff and alumni, as well as students assigned to other projects. Biweekly progress meetings were also held with ispace engineers, who reviewed progress and provided additional guidance.

Kickoff of the DSRP project officially began in March 2022, following approximately one year following initial contact, contract negotiations, and mission concept studies. Table 5 shows the progression of DSRP models throughout the entire design and implementation phase of the project. The first prototype of DSRP (Version 1)

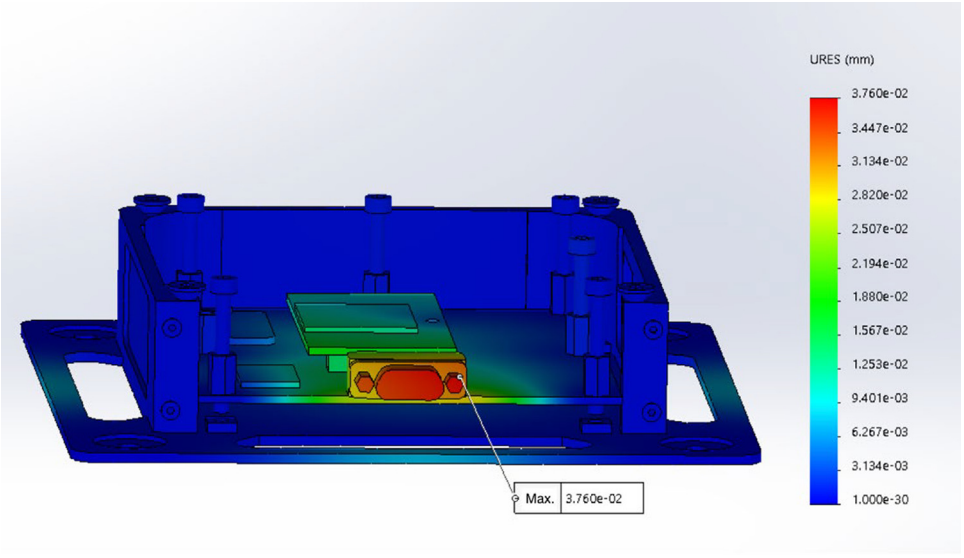

Fig. 8. Structural displacement of DSRP under random vibration conditions simulated by SolidWorks.

Table 5
Progression of DSRP models during the design and implementation process.

Version Number	Model	Completion Date	Notes
1	Prototype	2022/10	Basic circuit verification.
2	EM1	2023/01	Fit check with lander PIF. Increased test points on PCB.
3	EM2	2023/05	Increased baud rate. Qualification tests for vibration, shock, thermal vacuum, total ionizing dose, and single event effects. SOM chassis fixture modified.
4A	EM3	2023/07	Added watchdog IC and hard reset circuit.
4B	FM	2023/10	Removed hard reset circuit. Acceptance test for delivery.

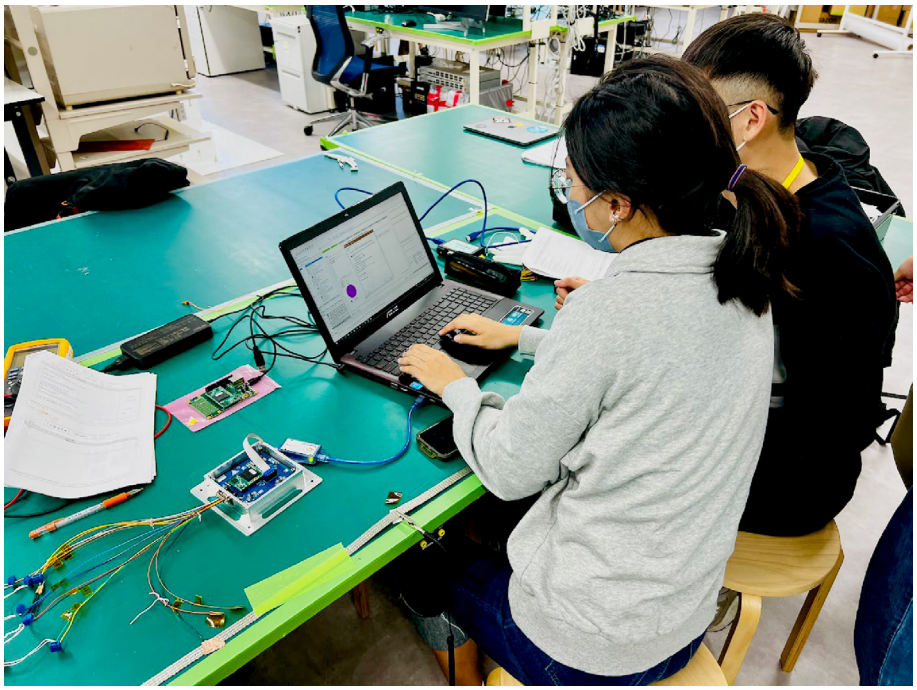

Fig. 9. Fit check between DSRP EM1 and the HAKUTO-R M2 PIF.

was completed in October 2022, allowing for verification and fault identification of the initial circuit designs, while also familiarizing members of the student team with the requisite design tools and methodology. Revisions based on these functional tests and verification were used to develop Version 2, which was the first EM (EM1) of DSRP. As shown in Fig. 9, DSRP EM1 was also subject to a fit check with the HAKUTO-R M2 PIF in February 2023 to verify the structural, data, and electrical interfaces between the payload and the lander.

Results from the fit check were used to produce DSRP Version 3 (EM2) in May 2023, which was the first revision of the payload to be subject to both functional and environmental testing. Environmental testing included shock, random vibration, sinusoidal vibration, quasi-static load, thermal vacuum, and ionizing radiation. The environmental tests were performed in this order, which is consistent with the expected lifecycle of the DSRP FM.

Based on discussions regarding the frequency of payload health monitoring and possible intervention by flight controllers, it was decided to implement watchdog functionality to DSRP Version 4A (EM3) to allow for autonomous recovery from software errors potentially caused by single event effects or shortcomings in payload embedded software design. The time available for troubleshooting and anomaly recovery is especially crucial during the period of alive time on the lunar surface, which is expected to be no longer than 12 days, making autonomous recovery a mission critical function. A watchdog IC capable of performing hard and soft resets of DSRP was included on Version 4A, with hard resets being performed after a threshold number of soft resets had occurred. The hard reset functionality was removed from Version 4B of DSRP, after it was verified that recovery from the software anomalies encountered during functional and environmental testing was possible using only a soft reset. Version 4B was selected as FM for the HAKUTO-R M2 mission and delivered to ispace in December 2023 for integration with the lander, which has been named Resilience (ispace inc., 2023a,b).

5.2. Vibration, load, and shock tests

Starting from DSRP Version 3, the payload was subject to vibration, load, and shock tests along all 3 axes (NASA Goddard Space Flight Center, 2005a,b; NASA, 1999) with specifications compliant with the IRD provided by ispace. After being secured to the vibration table on a fixture corresponding to the appropriate payload axis (Fig. 10), the payload was first subject to a resonance survey to verify that its normal modes were all larger than 140 Hz to avoid overlap with the normal modes of the launch vehicle engines. This was followed by a quasi-static load test by means of sine burst (EM only), sinusoidal vibration, random vibration, and another resonance survey to determine if the normal modes had shifted by over 10 % from pre-test values, indicating a non-negligible change in the payload structure possibly caused by deformation or separation. Finally, the DSRP Version 3 payload was subject to a shock test, followed by a final resonance survey to identify possible damage. The test levels for qualification and

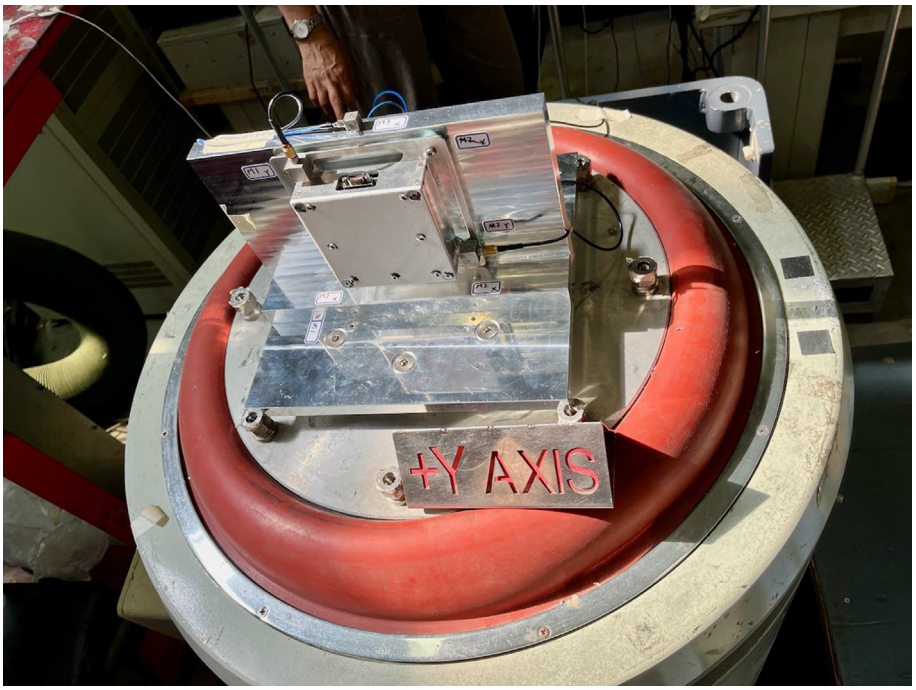

Fig. 10. DSRP secured to vibration table using fixture configuration for payload y-axis.

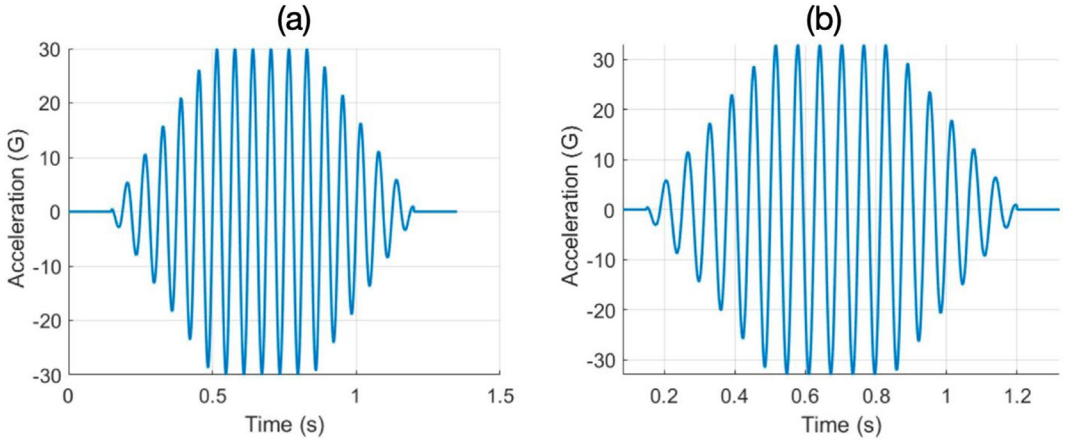

Fig. 11. Specification of sine burst qualification test along the DSRP (a) x- and y-axes, and (b) z-axis.

Table 6
Specifications of qualification level sinusoidal vibration test.

Frequency (Hz)	Level ($\times$9.8 m s^{-2})	Sweep Rate
2–25	±14.9 mm	2 octaves/minute
25–140	±24 mm	

acceptance testing were identical, except for random vibration where the acceptance levels were decreased by 3 dB.

The specifications of the sine burst tests used to qualify for quasi-static load are shown in Fig. 11. Consistent with the predicted environment for static acceleration, DSRP was subjected to sine burst tests with amplitudes of 30 g along the payload x- and y-axes (Fig. 11a) and 33 g along the payload z-axis (Fig. 11b). The time duration of the tests was approximately 1 s, but the loaded vibration table required pre-test warmups at amplitudes of 25 %, 50 %, and 75 % of the desired value before reaching the desired amplitude. As such, the DSRP models were subject to four quasi-static load tests of varying amplitudes on all three axes.

The specifications of the sinusoidal vibration qualification tests are shown in Table 6. Only the DSRP EMs were subject to sinusoidal vibration testing for qualification

purposes. The specifications of the random vibration qualification test used for the EMs were shown in Table 4. The acceptance levels used for the FM were 3 dB lower than the qualification levels. The shock test for the EM qualification tests had a shock response spectrum of 8 Gsrs at 100 Hz, as well as 1000 Gsrs at 1500 Hz and 10000 Hz. A shock test was not required for the FM.

The DSRP EMs and FMs all successfully passed the vibration, load, and shock tests, exhibiting consistency between pre and post-test normal modes and passing functional testing when powered on post-test. This verification has led to a high level of confidence that the DSRP FM can survive the mechanical stresses of the HAKUTO-R M2 flight environment.

5.3. Thermal vacuum cycling test (TVCT) and RADFET temperature coefficient characterization

The DSRP EMs and FM were all subject to thermal vacuum cycling testing (TVCT) to verify their ability to function in the expected on orbit and lunar surface environment (NASA Goddard Space Flight Center, 2005a,b). The control temperature selected for the TVCT was the temperature of the RADFET readout module, as the threshold voltage level of the RADFET used to infer ionizing radiation dose is sensitive to temperature. As shown in Fig. 12, the extreme control temperatures used for the hot and cold soaks were 60 °C and 0 °C, respectively. These correspond to the closest high value attainable using available test facilities to the worst case hot RADFET temperatures, as well as the lowest expected temperature considering the effect of the external heater installed on the lander side. The durations of the hot and cold soaks were 4 h.

As indicated by the red points in Fig. 12, two functional tests were performed at the beginning and end of each TVCT at ambient temperature, before and after pump down. The DSRP unit was powered off during the initial pump down, as well as during the final re-pressurization. The temperature cycles did not commence until after the first functional test after pump down was completed. The functional tests consisted of the transmission and verification of execution of a set of commands to DSRP involving telemetry requests and operational mode changes. A simplified set of commands was transmitted and verified during limited performance tests (LPTs) at the end of hot and cold soaks, as indicated by the green and yellow points in Fig. 12. An HK data request command was also transmitted to the DSRP unit every 30 s to verify payload aliveness. The configuration of the DSRP FM during TVCT is shown in Fig. 13. It can be seen that the MLI over the DSRP main body has been installed, although the MLI that will shield the harness to the lander was not installed for this test.

During the first TVCT for DSRP EM2, the test unit used was the one that experienced PCB warping during the bake out for epoxy curing as mentioned in the previous section. During the temperature reduction phases of the TVCT, the test unit became non-responsive to commands, while also showing anomalously large increases in electrical current. These anomalies occurred at temperatures similar to or lower than room temperature in the thermal vacuum chamber. Recovery was only possible by increasing the temperature with the test unit powered off and powering on again at room temperature. This anomaly was not reproducible using only cold sprays and refrigeration at normal atmospheric pressure but could be re-produced during a second TVCT with the same unit. Based on the hypoth-

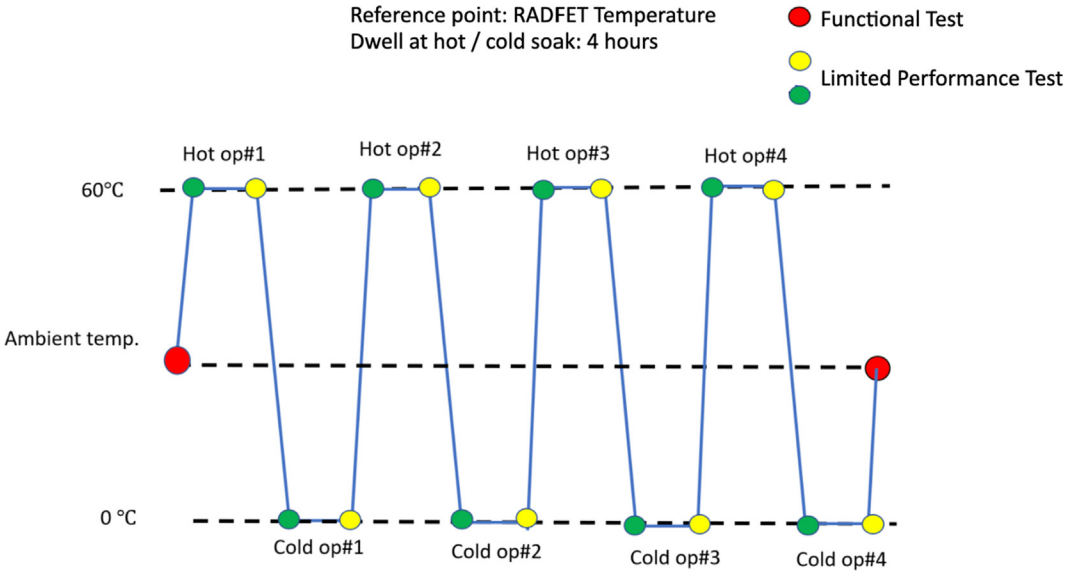

Fig. 12. Specifications of the acceptance level thermal vacuum cycling test for the DSRP FM. Temperature corresponds to that of the RADFET readout module, which was set as the control point.

esis that this anomaly was caused by damage to the PCB traces during the bake out, the configuration of the payload controller fastener was changed on subsequent test units as described in Section 4.2. This anomaly did not occur on subsequent test units with this modification.

The TVCT was also utilized to characterize the level of uncertainty in the measured radiation dose introduced by temperature variations of the RADFET readout module and associated electronics. For the batch of Varadis RM-VT01-A readout modules used for EM2, EM3, and the FM, the relation between the change in threshold voltage and accumulated radiation dose (*Dose*) for silicon in units of rad is:

$$\Delta V_{threshold} = A \times (Dose)^{B} \tag{1}$$

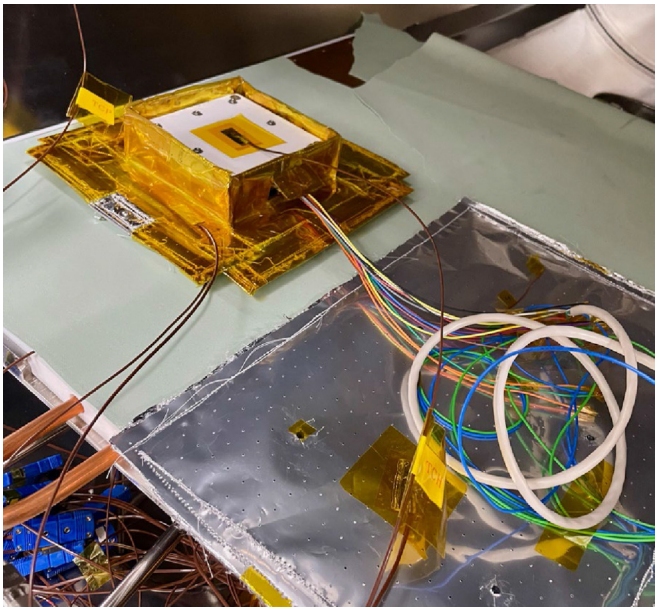

Fig. 13. Configuration of the DSRP FM (upper left) during TVCT. The payload harness providing power and data interfaces is visible extending from DSRP to the lower right.

Here for the dose range of 0 krad to 10 krad, $A = 0.0068$ and $B = 0.6164$ (Varadis, 2023). Solving for radiation dose:

$$Dose = \left(\frac{\Delta V_{threshold}}{A}\right)^{\frac{1}{B}} \tag{2}$$

The relation between uncertainty in inferred radiation dose ($\varepsilon(Dose)$) and uncertainty in threshold voltage ($\varepsilon(\Delta V_{threshold})$) can be derived through error propagation as:

$$\begin{aligned}\varepsilon(Dose) &= \sqrt{\left[\frac{\partial}{\partial \Delta V_{threshold}}\left(\frac{\Delta V_{threshold}}{A}\right)^{\frac{1}{B}}\right]^{2} \varepsilon(\Delta V_{threshold})^{2}} \\ &= \frac{1}{AB}\left(\frac{\Delta V_{threshold}}{A}\right)^{\frac{1-B}{B}} \varepsilon(\Delta V_{threshold})\end{aligned} \tag{3}$$

Fig. 14 shows the threshold voltages of RADFET R1 (a) and R2 (b) in the DSRP FM measured during the TVCT as a function of the RADFET temperature, as measured by the DSRP internal temperature sensor. It can be seen that the measured RADFET threshold voltages change very little with temperature, with R1 and R2 respectively showing mean threshold voltages of 1.40 V and 1.35 V. The standard deviation of the threshold voltages of R1 and R2 are respectively 2.52×10^{-3} V and 8.98×10^{-4} V. Taking these as the uncertainty in threshold voltage in Eq. (3), the resulting uncertainty in radiation dose as a result of these voltage fluctuations are respectively 16.55 rads and 5.77 rads, which is small compared to the survivable TID of 10 krad. This indicates that the relative uncertainty will be higher during earlier stages of the mission but will decrease along with the increasing TID throughout the course of the mission.

5.4. Ionizing radiation tests

The IRD provided by ispace for DSRP required that the payload be qualified to survive a total ionizing dose of 10

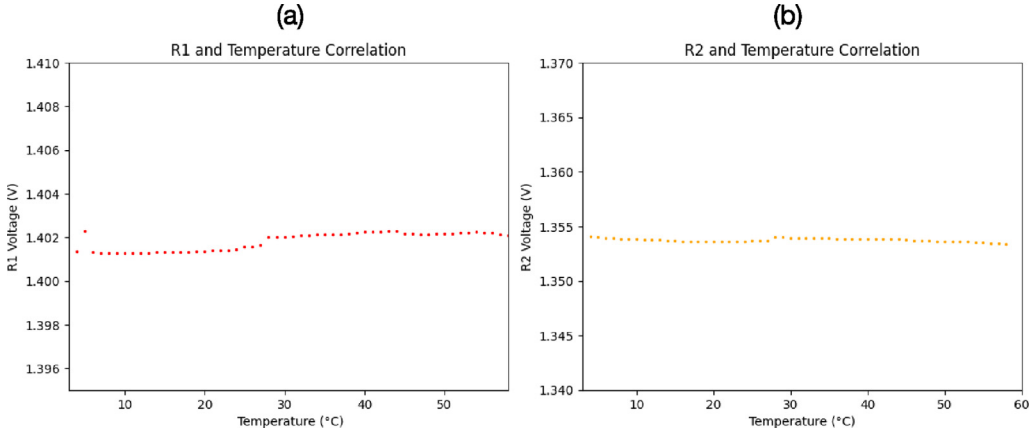

Fig. 14. Variation in threshold voltages of the DSRP FM RADFET R1 (a) and R2 (b) with control temperature during the TVCT.

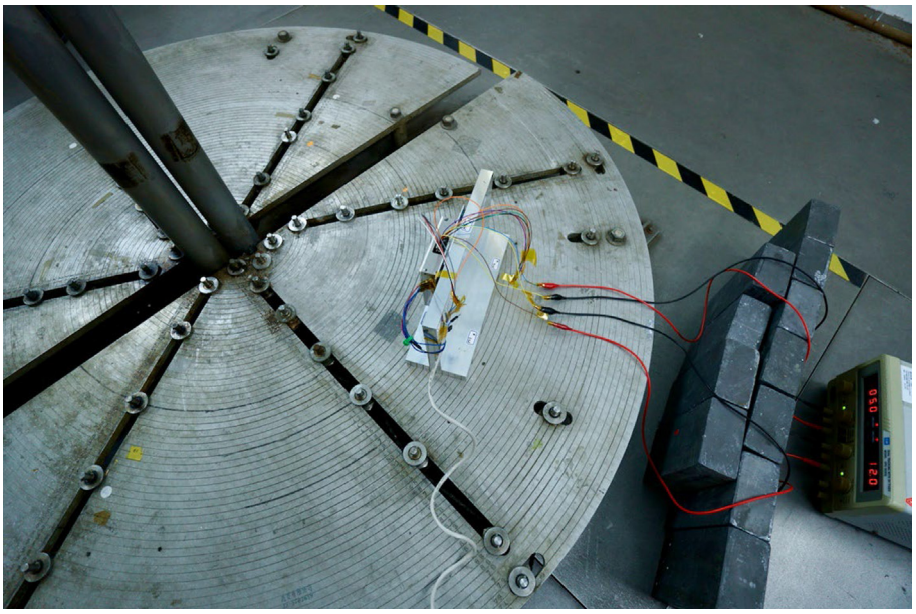

Fig. 15. Configuration of DSRP and fixture (center) during TID test. Cobalt-60 gamma ray source will be located at position of the two rods to the center left. Power supply behind lead castle shielding is at the lower right.

krad with aluminum shielding of 1 mm. Starting from Version 3, DSRP was subject to total ionizing dose (TID) tests to verify its ability to survive the required TID, as well as to characterize the radiation doses inferred from the measured RADFET threshold voltages. The ability to recover from single event effects and identify bit flips in NAND Flash for the SEU counting experiment was also verified using a proton beam to simulate the effects of cosmic ray proton strikes. DSRP units subject to radiation tests were disqualified from flight.

A qualification unit using Version 3 of DSRP (EM2) was subject to two rounds of TID testing using a Cobalt-60 gamma ray source operated by the Institute of Nuclear Engineering and Science at National Tsing Hua University (NTHU). There was a 16 day interval between the tests. In both tests, the DSRP qualification unit was attached to a fixture located 40 cm from the gamma ray source, as shown in Fig. 15. The dose rate provided by NTHU was taken as ground truth, with a value of 2.48 krad hour^{-1} (24.8 Grey hour^{-1}). During the tests, the DSRP unit was powered on

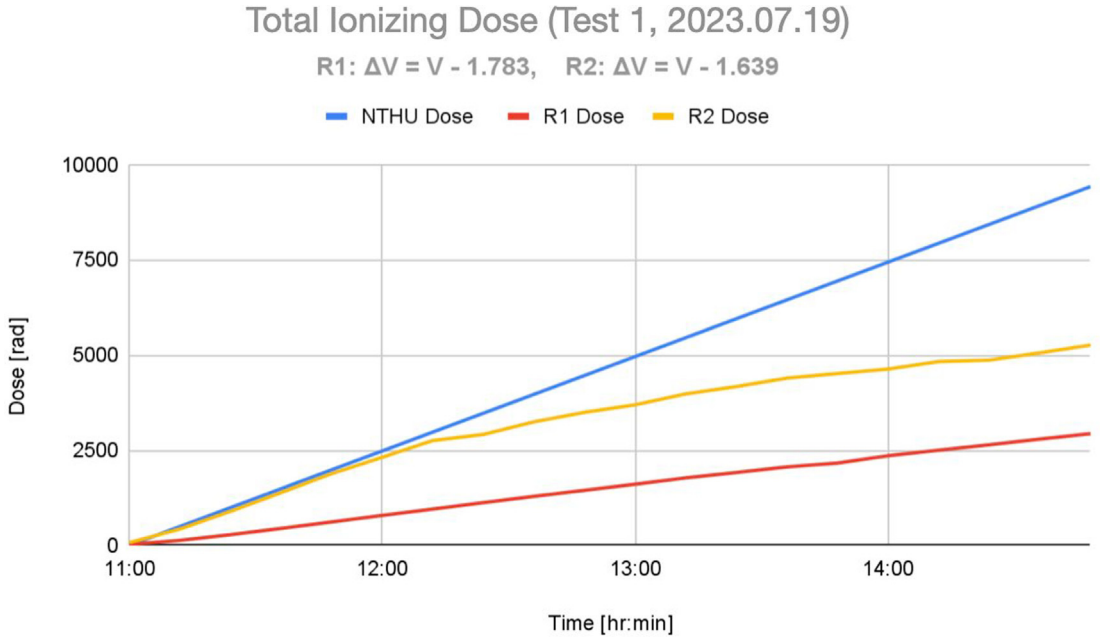

Fig. 16. Time variation of ionizing dose inferred from threshold voltage changes of RADFET R1 (red line), R2 (orange line), and the dose rate provided by NTHU considered as calibrated data (blue line). The time corresponds to the local time at which the test was conducted.

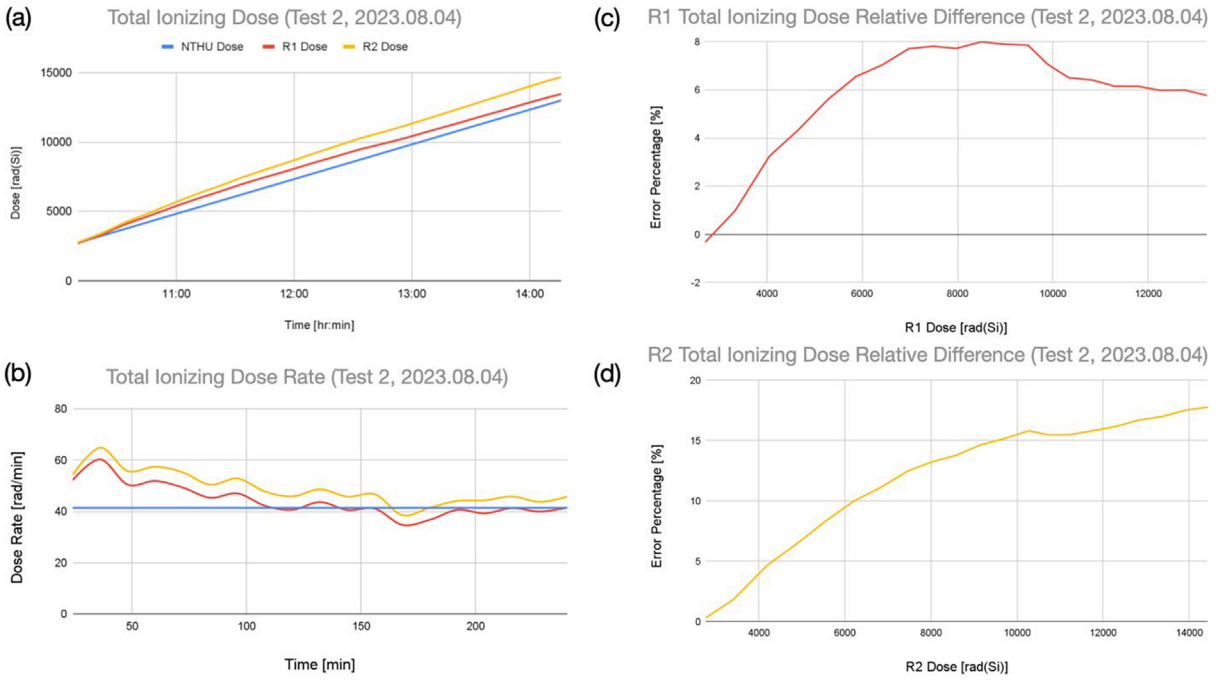

Fig. 17. (a) Time variation in total ionizing dose inferred from RADFET R1 (red line), R2 (orange line), and NTHU dose rate. Time is given as local time during which the test was conducted. (b) Time variation in total ionizing dose rate inferred from RADFET R1 (red line) and R2 (orange line), compared with NTHU supplied dose rate (blue line). Time is denoted as time elapsed since the start of the test. (c) Relative difference between RADFET R1 total ionizing dose and dose computed using NTHU dose rate. (d) Same as (c), but for RADFET R2.

and continuously commanded to return HK telemetry every 30 s, allowing the R1 and R2 RADFET threshold voltages to be monitored. The first test was 3 h and 48 min in duration, corresponding to a dose of 9.424 krad. The second test was 4 h and 6 min in duration, corresponding to a dose of 10.168 krad. The unit thus accumulated a total dose of 19.592 krad before experiencing a component failure at the end of the second test, namely the 3.3 V DC-DC converter. Since this TID exceeded the maximum TID survivability requirement of 10 krad, replacement was not deemed to be nessecary.

The two separate TID tests also allowed for operational factors in the payload embedded software affecting the inferred radiation dose to be identified. Fig. 16 shows the time variation of total ionizing dose inferred from the threshold voltage changes in RADFET R1 (red line) and R2 (orange line) using Equation (1) compared with the dose computed using the dose rate provided by NTHU (blue line). The time corresponds to the local time during which the experiment was performed. For the purposes of the radiation tests, the NTHU dose is considered to be calibrated data. The discrepancy between the inferred doses and the calibrated dose is significant with R1, which consistently shows a relative error on the order of 70 %. The dose error from R1 is initially lower, with values on the order of 10 % during the first hour of the test, but rapidly increases thereafter, growing to 40 % by the end of the test. After consultations with Varadis, it was determined that the cause of this discrepancy was the fact that

Fig. 18. Configuration of DSRP test unit during SEE test. Center target of proton beam illuminated by laser cross hairs.

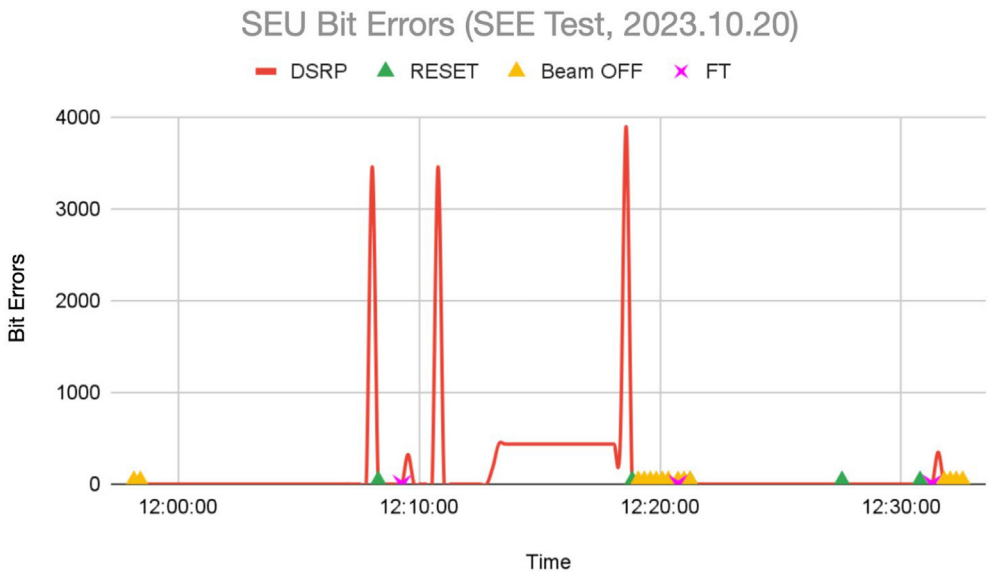

Fig. 19. Number of bit errors detected in DSRP NAND Flash as a function of local time during the SEE test (red line). Green triangles denote commanded resets of DSRP, orange triangles denote times when the proton beam was switched off, pink stars denote times when functional tests were performed on the DSRP test unit.

the RADFET readout module was continuously kept in read out mode during the operation of DSRP, resulting in decreased sensitivity to ionizing radiation.

Based on these results, the DSRP embedded software was modified such that the RADFET readout module was kept in irradiation mode with all control pins grounded when not actively being polled for threshold voltage readings by the payload controller. This results in the RADFET readout module being in readout mode for less than 1 s during each reading. Test 2 was performed using this new configuration. Fig. 17a shows the time variation of the total ionizing dose inferred from RADFET R1 (red line) and R2 (orange line), compared with the dose computed using the NTHU supplied dose rate (blue line), which is again considered to be calibrated data for the purposes of this test. Note that the total ionizing dose does not start from 0 rads due to the change in RADFET threshold voltages from Test 1. Compared to Test 1, the RADFET inferred total ionizing dose curves are much closer to that of the truth data. A similar situation can be seen for the dose rates computed from the RADFET observations shown in Fig. 17b. From the relative differences between the RADFET R1 and R2 and truth total ionizing doses shown respectively in Fig. 17c and d, it can be seen that the total ionizing dose inferred from R1 showed a maximum difference of 8 % from the truth values, while R2 showed a maximum difference of 17 %. Additional TID tests will be performed to determine the consistency of these results for other RM-VT01-A RADFET readout modules from the same production batch, to aid in data calibration.

A proton beam was used to bombard a DSRP Version 4A (EM3) test unit to simulate single event effects (SEEs) caused by cosmic ray strikes. The objective was to verify the ability of DSRP to survive and recover from SEE, while also verifying the ability of DSRP to detect and count bit errors in the onboard NAND Flash as required by the SEU counting experiment. The test setup utilized the proton beam produced by a 230 MeV cyclotron at the Proton and Radiation Therapy Center of Linkou Chang Gung Memorial Hospital (Hsiao et al., 2024). The proton beam had a mean energy of 221.2 MeV, with a proton flux of 1.32×10^7 cm^2 s^{-1}. A broad beam in the shape of an 8 cm $\times$ 8 cm square was used to irradiate the bare DSRP PCB board, which was powered on during the entire duration of the test. The beam was targeted on a point just adjacent to the payload controller, as shown in Fig. 18.

During the SEE test, the DSRP test unit was irradiated by the proton beam for a total time of 33 min, resulting in a fluence of 2.37×10^{10} cm^{-2} and an estimated dose of 1.29 krad. The test unit was polled for housekeeping data every 15 min and also periodically subjected to functional tests and commanded resets. The SEU counting experiment was performed using a total memory volume of 3.78 MB. No anomalous un-commanded resets or power cycles occurred during the test, which indicates that embedded software hangs, as well as power cycling to recover from SEL induced overcurrent events did not occur, verifying the ability of DSRP to tolerate proton strikes.

The red line in Fig. 19 shows the number of bit errors detected in DSRP NAND Flash during the SEE test as a function of local time. It can be seen that there were five distinct spikes in bit errors during the periods of irradiation. Given that similar spikes in bit errors were not produced during the operation of DSRP for equal or longer periods of time while not being irradiated, these bit errors are likely the result of SEUs caused by proton bombardment. This provides confidence that DSRP is capable of

detecting bit errors caused by proton strikes. One anomalous point is the persistence of 436 bit errors for a 5 min period starting around 12:13 local time. This may be attributable to a software bug, as the bits in error should be reset at the end of each memory sweep. Another possibility is a charge pump failure, which can prevent a proper erase from occurring. The cause for this bug is still under investigation, but similar persistent events can be identified and corrected during post-processing.

6. Discussion and future work

Following acceptance testing, the DSRP FM for HAKUTO-R Mission 2 was delivered to ispace for integration with the Resilience lunar lander in December 2023. As delivered, the DSRP FM had a total mass of 399 g. Of this, the chassis and PCB comprising the main body of the payload accounted for 342 g, while MLI covering the main body and the harnessing accounted for 57 g. HAKUTO-R Mission 2 is scheduled for launch no earlier than Q4 2024. DSRP is expected to be powered on shortly after launch with the opportunity to begin measurements as the spacecraft passes through the Van Allen Belts. DSRP is expected to be active during Earth-Moon transit, in lunar orbit, as well as on the lunar surface.

DSRP Version 4B units with the same configuration as the FM are being used on the ground by ispace and NCU for simulation and diagnostic purposes during spacecraft integration and the mission. Additional TID tests will be performed to examine the consistency of differences between radiation doses measured by DSRP and truth values, in order to generate correction factors that can be used in the calibration of flight data. Due to the accelerated development schedule and the learning curve for FPGA and software design required, some shortcomings in the payload software development were addressed by treating symptoms rather than the root cause. For example: a data read anomaly that consistently occurred after long term operation of DSRP was treated by forcing periodic autonomous soft resets. Additional diagnostic and debugging work will be performed to identify the cause and a more robust solution for future revisions. The SEU counting algorithm will also be revised to use a more realistic mix of 1 s and 0 s, as opposed to the current version which uses only 1 s.

The form factor and interface of DSRP is also being modified to be compatible with the 3U CubeSat form factor of the COSPAR-1 mission, which is in development as a Low Earth Orbit kickoff mission for the Committee on Space Research (COSPAR) Task Group on Establishing a Constellation of Small Satellites (TGCSS) tentatively scheduled for the late 2024/early 2025 time period (Baker et al., 2020; Smallsat News, 2023). The low mass, power consumption, data size, and pointing requirements of the revised version of DSRP, named the Compact Radiation Probe (CRP), make it particularly attractive for CubeSat use.

7. Conclusions

In this study, we have examined the scientific and capacity building motivations behind the development of the Deep Space Radiation Probe to be flown aboard the ispace HAKUTO-R M2 commercial lunar lander scheduled for launch in late 2024. Considering the rapid growth of lunar exploration, rideshare opportunities, and infrastructure development, the mission is motivated by the need to better characterize the ionizing radiation environment between the Earth and the Moon, as well as to develop the capacity to design and implement payloads and spacecraft systems for the deep space environment. The rapid design and implementation process by an NCU student team over the course of a 21-month period has been described, which provided a valuable hands-on education opportunity, while also serving to establish deep space design and exploration capacity. The ionizing radiation dose, dose rate, and SEU bit error count data products that will be produced by DSRP aboard the HAKUTO-R M2 Resilience lander will be beneficial in characterizing the deep space radiation environment at a time of growing activity in this region.

CRediT authorship contribution statement

Loren C. Chang: Writing – review & editing, Writing – original draft, Visualization, Validation, Supervision, Resources, Project administration, Methodology, Investigation, Funding acquisition, Formal analysis, Conceptualization. **Wei-Yi Lin:** Software, Methodology, Investigation, Formal analysis, Conceptualization. **Yi-Hsuan Chou:** Visualization, Validation, Software, Methodology, Investigation, Formal analysis, Data curation. **Jen-Siang Lin:** Visualization, Validation, Resources, Methodology, Investigation, Formal analysis, Conceptualization. **Chieh Lung:** Visualization, Validation, Methodology, Investigation, Formal analysis. **I. Chen:** Validation, Software, Formal analysis. **Kai-Jie Hou:** Visualization, Validation, Methodology, Investigation, Conceptualization. **Glenn Franco Gacal:** Methodology, Investigation. **Yi-Chung Chiu:** Supervision, Resources, Project administration, Methodology. **Yushun Wang:** Software, Resources, Methodology. **Hui-Hui Chou:** Methodology, Investigation, Formal analysis. **Chi-Kuang Chao:** Validation, Resources. **Jann-Yenq Liu:** Resources, Funding acquisition. **Tung-Yuan Hsiao:** Validation, Resources. **I-Chun Cho:** Validation, Resources. **Takumi Date:** Supervision, Resources. **Masayuki Urata:** Supervision, Resources. **Masahiro Taeda:** Supervision, Resources. **Kenichiro Tanaka:** Supervision, Resources. **Nikola Vasovic:** Methodology. **Niall Keegan:** Methodology.

Declaration of competing interest

The authors declare the following financial interests/personal relationships which may be considered as potential

competing interests: "Loren C. Chang reports financial support was provided by National Science and Technology Council, Taiwan. Loren C. Chang reports financial support was provided by Ministry of Education, Taiwan".

Acknowledgements

This research was funded by financial support from President Jing-Yang Jou of National Central University, as well as generous donations from private individuals and companies to the NCU Endowment Fund. Additional support was provided by grants 111-2636-M-008-004 and 112-2636-M-008-003 from the Taiwan National Science and Technology Council to L.C. Chang, as well as the Higher Education SPROUT grant from the Taiwan Ministry of Education to the NCU Center for Astronautical Physics and Engineering. The Authors thank Bill Chang of HelioX Cosmos for support throughout this project, Rafael Yuwei Li for student mentoring, as well as support for project kickoff in 2021 from the Taoyuan City Government under the administration of Mayor Wen-Tsan Cheng. L.C. Chang thanks grant 113-2111-M-008-007 from the Taiwan National Science and Technology Council and Sophie Kimura of Kyushu University for ongoing work on the development of the Compact Radiation Probe, the Taiwan Space Union for discussions on lunar science, and Taiwan Space Generation for collaborations on popular space outreach and professional development.

References

Andjelkovic, M., Simevski, A., Chen, J., et al., 2022. A design concept for radiation hardened RADFET readout system for space applications. Microprocess. Microsyst. 90104486.

Baker, D.N., 2000. The occurrence of operational anomalies in spacecraft and their relationship to space weather. IEEE Trans. Plasma Sci. 28 (6), 2007–2016.

Baker, D., Chandran, A., Chang, L., et al., 2020. An international constellation of small spacecraft. Space Res. Today 208, 23–28.

Baumann, R., Kruckmeyer, K., 2019. Radiation Handbook for Electronics. Texas Instruments Incorporated, Dallas, TX.

Chandran, A., Fang, T.-W., Chang, L., et al., 2021. The INSPIRESat-1: Mission, science, and engineering. Adv. Space Res. 68, 2616–2630. https://doi.org/10.1016/j.asr.2021.06.025.

Chen, J., Andjelkovic, M., Simevski, A., et al., 2019. Design of SRAM-based Low-Cost SEU Monitor for Self- Adaptive Multiprocessing Systems. Kallithea, Greece, s.n., pp. 514–521. https://doi.org/10.1109/DSD.2019.00080.

Chern, J.-S., Wu, A.-M., Lin, S.-F., 2006. Lesson learned from FORMOSAT-2 mission operations. Acta Astronaut. 59 (1–5), 344–350.

Chiu, Y.C., Chang, L.C., Chao, C.K., et al., 2022. Lessons learned from IDEASSat: Design, testing, on orbit operations, and anomaly analysis of a first University CubeSat intended for ionospheric science. Aerospace 9 (110). https://doi.org/10.3390/aerospace9020110.

Desai, M.I., Allegrini, F., Ebert, R.W., et al., 2019. The CubeSat mission to study solar particles. IEEE Aerosp. Electron. Syst. Mag. 34 (4), 16–28.

Duann, Y., Chang, L.C., Chao, C.-K., et al., 2020. IDEASSat: A 3U CubeSat mission for ionospheric science. Adv. Space Res. 66, 116–134. https://doi.org/10.1016/j.asr.2020.01.012.

Eastes, R.W., McClintock, W.E., Burns, A.G., et al., 2017. The global-scale observations of the limb and disk (GOLD) mission. Space Sci. Rev. 212, 383–408. https://doi.org/10.1007/s11214-017-0392-2.

Fabiano, M., Furano, G., 2013. NAND flash storage technology for mission-critical space applications. IEEE Aerosp. Electron. Syst. Mag. 28 (9), 30–36.

Heidecker, J., 2012. NAND flash screening and qualification guideline for space application. [Online] Available at: https://dataverse.jpl.nasa.gov/dataset.xhtml?persistentId=hdl:2014/41965 [Accessed 21 December 2023].

Hsiao, T.Y., Wang, L.K., Chen, T.Y., et al., 2024. Proton FLASH irradiation platform for small animal setup at Chang Gung Memorial Hospital. IEEE Trans. Radiat. Plasma Med. Sci. 8 (1), 88–94.

ispace inc., 2023b. ispace Releases Updates on Progress of Mission 2 and Mission 3. [Online] Available at: https://ispace-inc.com/news-en/?p=4401 [Accessed 21 December 2023].

ispace inc., 2023a. ispace Announces Mission 2 with Unveiling of Micro Rover Design. [Online] Available at: https://ispace-inc.com/news-en/?p=4954 [Accessed 7 January 2024].

Langley, T., Koga, R., Morris, T., 2003. Single-event effects test results of 512MB SDRAMs. In: 2003 IEEE Radiation Effects Data Workshop, Monterey, CA, USA, 25–25 July. https://doi/org/10.1109/REDW.2003.1281355.

Lin, Z., Chao, C.K., Liu, J.Y., et al., 2017. Advanced ionospheric probe scientific mission onboard FORMOSAT-5 satellite. Terr. Atmos. Ocean. Sci. 28, 99–110. https://doi.org/10.3319/TAO.2016.09.14.01(EOF5).

Maltagliati, L., 2023. A long-awaited return to the Moon. Nat. Astron 22 December, 10. https://doi.org/10.1038/s41550-022-01877-8.

Microchip Technology, Inc., 2023. SmartFusion 2 FPGAs. [Online] Available at: https://www.microchip.com/en-us/products/fpgas-and-plds/system-on-chip-fpgas/smartfusion-2-fpgas [Accessed 28 December 2023].

Micron Technology, Inc., 2023. MT29F128G08AJAAAWP-ITZ. [Online] Available at: https://www.mouser.tw/datasheet/2/671/micron_technology_micts06235-1-1759187.pdf [Accessed 21 December 2023].

Microsemi, 2014. IGLOO2 and Smart Fusion2 65nm Commercial Flash FPGAs Interim Summary of Radiation Test Results. [Online] Available at: https://www.microsemi.com/document-portal/doc_download/134103-igloo2-and-smartfusion2-fpgas-interim-radiation-report [Accessed 7 January 2024].

Millan, R.M., von Steiger, R., Ariel, M., et al., 2019. Small satellites for space science: A COSPAR scientific roadmap. Adv. Space Res. 64 (8), 1466–1517.

Mitchao, D.P., Totani, T., Wakita, M., Nagata, H., 2018. Preliminary thermal design for microsatellites deployed from International Space Station's Kibo Module. J. Thermophys Heat Transfer 32 (3), 789–798.

NASA Goddard Space Flight Center, 2005. Structural and Mechanical. In: General Environmental Verification Standard (GEVS) for GSFC Flight Programs and Projects. NASA Goddard Space Flight Center, Greenbelt (MD), pp. 2.4-1–2.4-27.

NASA Goddard Space Flight Center, 2005. Thermal-Vacuum Qualification. In: General Environmental Verification Standard (GEVS) for GSFC Flight Programs and Projects. NASA Goddard Space Flight Center, Greenbelt (MD), pp. 2.6-1–2.6-12.

NASA, 1999. Reliability Preferred Practice PT-TE-1420 Sine-Burst Load Test. [Online] Available at: https://extapps.ksc.nasa.gov/Reliability/Documents/Preferred_Practices/1420.pdf [Accessed 8 January 2024].

NASA, 2003. EEE-INST-002: Instructions for EEE Parts Selection, Screening, Qualification, and Derating. [Online] Available at: https://nepp.nasa.gov/index.cfm/12821 [Accessed 9 January 2024].

Rodbell, K.P., Heidel, D.F., Tang, H.H.K., et al., 2007. Low-energy proton-induced single-event-upsets in 65 nm node, silicon-on-insulator, latches and memory cells. IEEE Trans. Nucl. Sci. 54 (6), 2474–2479.

Sheng, J., Qiu, M., Xu, P., et al., 2024. Estimation method for bit upset ratio of NAND flash memory induced by heavy ion irradiation. AIP Adv. 14 (025124), 1–8.

Sinclair, D., Dyer, J., 2013. Radiation Effects and COTS Parts in SmallSats. Utah State University, Logan, Utah, USA.

Smallsat News, 2023. The COSPAR satellite for advanced Earth science research enjoys collaboration from 5 countries. [Online] Available at: https://smallsatnews.com/2023/05/18/the-cospar-satellite-for-advanced-earth-science-research-enjoys-collaboration-from-5-countries/ [Accessed 11 January 2024].

SpaceX, 2023. Rideshare Payload User's Guide, Version 9. [Online] Available at: https://storage.googleapis.com/rideshare-static/Rideshare_Payload_Users_Guide.pdf [Accessed 6 January 2024].

Tsiligiannis, G., Danzeca, S., 2017. SmartFusion2 and Artix 7 radiation test results for the new developments. [Online] Available at: https://indico.cern.ch/event/608587/contributions/2712676/attachments/1523165/2380407/FPGA_TWEPP2017.pptx [Accessed 8 April 2024].

Varadis, 2022. TECHNICAL DATA VT01 400nm RADFET in 6L SOT-23 Plastic package. [Online] Available at: https://www.varadis.com/wp-content/uploads/2022/04/VT01-Datasheet_rev2p2.pdf [Accessed 21 December 2023].

Varadis, 2023. C of C/Test Data Record, RM-VT01-A-L4, P5925W3, s.l.: s.n.

Wertz, J.R., Larson, W.J., 1999. Space Mission Analysis and Design, third ed. Microcosm Press, Hawthorne, CA.